EUROPEAN ORGANISATION FOR NUCLEAR RESEARCH (CERN)

Submitted to: Phys. Rev. D

CERN-EP-2018-099
May 11, 2018

Measurements of total production cross sections for π^++C, π^++Al, K^++C, and K^++Al at 60 GeV/c and π^++C and π^++Al at 31 GeV/c

The NA61/SHINE Collaboration

The NA61/SHINE Collaboration

A. Aduszkiewicz[18], E. Andronov[24], T. Antićić[3], N. Antoniou[8], B. Baatar[22], M. Baszczyk[16], S. Bhosale[13], A. Blondel[26], M. Bogomilov[2], A. Brandin[23], A. Bravar[26], W. Bryliński[20], J. Brzychczyk[15], S.A. Bunyatov[22], O. Busygina[21], A. Bzdak[16], S. Cao[10], H. Cherif[7], P. Christakoglou[8], M. Ćirković[25], T. Czopowicz[20], A. Damyanova[26], A. Datta[30], N. Davis[13], M. Deveaux[7], F. Diakonos[8], P. von Doetinchem[30], W. Dominik[18], P. Dorosz[16], J. Dumarchez[4], R. Engel[5], G.A. Feofilov[24], L. Fields[27], M. Friend[10], Z. Fodor[9,19], A. Garibov[1], M. Gaździcki[7,12], O. Golosov[23], M. Golubeva[21], K. Grebieszkow[20], F. Guber[21], A. Haesler[26], T. Hasegawa[10], A.E. Hervé[5], S. Igolkin[24], A. Ivashkin[21], S.R. Johnson[29], K. Kadija[3], A. Kapoyannis[8], E. Kaptur[17], N. Kargin[23], E. Kashirin[23], M. Kiełbowicz[13], V.A. Kireyeu[22], V. Klochkov[7], T. Kobayashi[10], V.I. Kolesnikov[22], D. Kolev[2], A. Korzenev[26], V.N. Kovalenko[24], K. Kowalik[14], S. Kowalski[17], M. Koziel[7], A. Krasnoperov[22], W. Kucewicz[16], M. Kuich[18], A. Kurepin[21], D. Larsen[15], A. László[9], T.V. Lazareva[24], M. Lewicki[19], K. Łojek[15], B. Łysakowski[17], V.V. Lyubushkin[22], M. Maćkowiak-Pawłowska[20], Z. Majka[15], B. Maksiak[20], A.I. Malakhov[22], D. Manić[25], A. Marchionni[27], A. Marcinek[13], A.D. Marino[29], K. Marton[9], H.-J. Mathes[5], T. Matulewicz[18], V. Matveev[22], G.L. Melkumov[22], A. Merzlaya[15], B. Messerly[31], Ł. Mik[16], G.B. Mills[28], S. Morozov[21,23], S. Mrówczyński[12], Y. Nagai[29], T. Nakadaira[10], M. Naskręt[19], V. Ozvenchuk[13], A.D. Panagiotou[8], V. Paolone[31], M. Pavin[4,3], O. Petukhov[21], R. Płaneta[15], P. Podlaski[18], B.A. Popov[22,4], M. Posiadała[18], S. Puławski[17], J. Puzović[25], W. Rauch[6], M. Ravonel[26], R. Renfordt[7], E. Richter-Wąs[15], D. Röhrich[11], E. Rondio[14], M. Roth[5], B.T. Rumberger[29], A. Rustamov[1,7], M. Rybczynski[12], A. Rybicki[13], A. Sadovsky[21], K. Sakashita[10], K. Schmidt[17], T. Sekiguchi[10], I. Selyuzhenkov[23], A.Yu. Seryakov[24], P. Seyboth[12], A. Shukla[30], M. Słodkowski[20], A. Snoch[7], P. Staszel[15], G. Stefanek[12], J. Stepaniak[14], M. Strikhanov[23], H. Ströbele[7], T. Šuša[3], M. Tada[10], A. Taranenko[23], A. Tefelska[20], D. Tefelski[20], V. Tereshchenko[22], A. Toia[7], R. Tsenov[2], L. Turko[19], R. Ulrich[5], M. Unger[5], F.F. Valiev[24], M. Vassiliou[8], D. Veberič[5], V.V. Vechernin[24], M. Walewski[18], A. Wickremasinghe[31], Z. Włodarczyk[12], A. Wojtaszek-Szwarc[12], O. Wyszyński[15], K. Yarritu[28], L. Zambelli[4,10], E.D. Zimmerman[29], and R. Zwaska[27]

[1] National Nuclear Research Center, Baku, Azerbaijan
[2] Faculty of Physics, University of Sofia, Sofia, Bulgaria
[3] Ruđer Bošković Institute, Zagreb, Croatia
[4] LPNHE, University of Paris VI and VII, Paris, France
[5] Karlsruhe Institute of Technology, Karlsruhe, Germany
[6] Fachhochschule Frankfurt, Frankfurt, Germany
[7] University of Frankfurt, Frankfurt, Germany
[8] University of Athens, Athens, Greece
[9] Wigner Research Centre for Physics of the Hungarian Academy of Sciences, Budapest, Hungary
[10] Institute for Particle and Nuclear Studies, Tsukuba, Japan
[11] University of Bergen, Bergen, Norway
[12] Jan Kochanowski University in Kielce, Poland
[13] H. Niewodniczański Institute of Nuclear Physics of the Polish Academy of Sciences, Kraków, Poland
[14] National Centre for Nuclear Research, Warsaw, Poland
[15] Jagiellonian University, Cracow, Poland
[16] University of Science and Technology, Cracow, Poland
[17] University of Silesia, Katowice, Poland
[18] University of Warsaw, Warsaw, Poland
[19] University of Wrocław, Wrocław, Poland
[20] Warsaw University of Technology, Warsaw, Poland

[21] Institute for Nuclear Research, Moscow, Russia
[22] Joint Institute for Nuclear Research, Dubna, Russia
[23] National Research Nuclear University (Moscow Engineering Physics Institute), Moscow, Russia
[24] St. Petersburg State University, St. Petersburg, Russia
[25] University of Belgrade, Belgrade, Serbia
[26] University of Geneva, Geneva, Switzerland
[27] Fermilab, Batavia, USA
[28] Los Alamos National Laboratory, Los Alamos, USA
[29] University of Colorado, Boulder, USA
[30] University of Hawaii at Manoa, USA
[31] University of Pittsburgh, Pittsburgh, USA

This paper presents several measurements of total production cross sections and total inelastic cross sections for the following reactions: π^{+}+C, π^{+}+Al, K^{+}+C, K^{+}+Al at 60 GeV/c, π^{+}+C and π^{+}+Al at 31 GeV/c. The measurements were made using the NA61/SHINE spectrometer at the CERN SPS. Comparisons with previous measurements are given and good agreement is seen. These interaction cross sections measurements are a key ingredient for neutrino flux prediction from the reinteractions of secondary hadrons in current and future accelerator-based long-baseline neutrino experiments.

1 Introduction

The NA61 or SPS Heavy Ion and Neutrino Experiment (SHINE) [1] at the CERN Super Proton Synchrotron (SPS) has a broad physics program that includes heavy ion physics, cosmic ray physics, and neutrino physics. Long-baseline neutrino beams are typically initiated by high-energy protons that strike a long target, yielding hadrons that can decay to neutrinos or can reinteract in the target or in the aluminum focussing horns, potentially producing additional neutrino-yielding hadrons. NA61/SHINE has already been very successful at measuring the yields of secondary hadrons generated by 31 GeV/c protons on carbon targets [2, 3] for the Tokai-to-Kamioka (T2K) long-baseline neutrino oscillation experiment [4]. Data at higher energies are now being collected to benefit other neutrino experiments, particularly MINERνA [5], NOνA [6] that use the current NuMI neutrino beamline at Fermilab, and the proposed DUNE experiment [7] which will use the planned LBNF beamline. The NuMI beamline is initiated by 120 GeV/c protons on a carbon target, while LBNF will use 60-120 GeV/c protons on a carbon or beryllium target.

During the fall of 2015, NA61/SHINE recorded interactions of positively charged protons, pions, and kaons on thin carbon and aluminum targets. In the case of pions, interactions were recorded at beam momenta of 31 GeV/c and 60 GeV/c. Kaons were recorded with a beam momentum of 60 GeV/c only, and protons at 31 GeV/c only. The NA61/SHINE vertex magnets were not operational during this period. Therefore, final state particles could not be identified and spectral measurements could not be extracted from this data run. As a result of this setup, data-taking was optimized for making measurements of the total production and total inelastic cross sections for each interaction.

The total cross section of hadron-nucleus interactions σ_{tot} can be defined in terms of the inelastic σ_{inel} and coherent elastic σ_{el} cross sections:

$$\sigma_{\mathrm{tot}} = \sigma_{\mathrm{inel}} + \sigma_{\mathrm{el}}. \tag{1}$$

The inelastic cross section σ_{inel} is defined as the sum of all processes due to strong interactions except coherent nuclear elastic scattering. The production processes are defined as those in which new hadrons are produced. The inelastic processes additionally include interactions which only result in the disintegration of the target nucleus (quasi-elastic interactions). Taking into account quasi-elastic scattering as a subset of the inelastic scattering process, one can define the production cross section σ_{prod} in terms of the quasi-elastic cross section σ_{qe} as:

$$\sigma_{\mathrm{prod}} = \sigma_{\mathrm{inel}} - \sigma_{\mathrm{qe}}. \tag{2}$$

This paper is organized as follows: Section 2 describes the experimental apparatus. Section 3 presents the event selection to ensure the quality of the measurements. Section 4 presents the procedure for measuring σ_{inel} and σ_{prod} cross sections. Section 5 describes the corrections to the raw trigger probability. Section 6 discusses systematic uncertainties. The final results and discussion are presented in Sections 7 and 8.

2 Experimental setup, Beams, and Data Collected

NA61/SHINE receives a secondary hadron beam from the 400 GeV/c SPS proton beam. The primary proton beam strikes a beryllium target 535 m upstream generating the secondary beam. A magnet system is then used to select the desired beam momentum. Unwanted positrons and electrons are absorbed by two 4 mm lead absorbers.

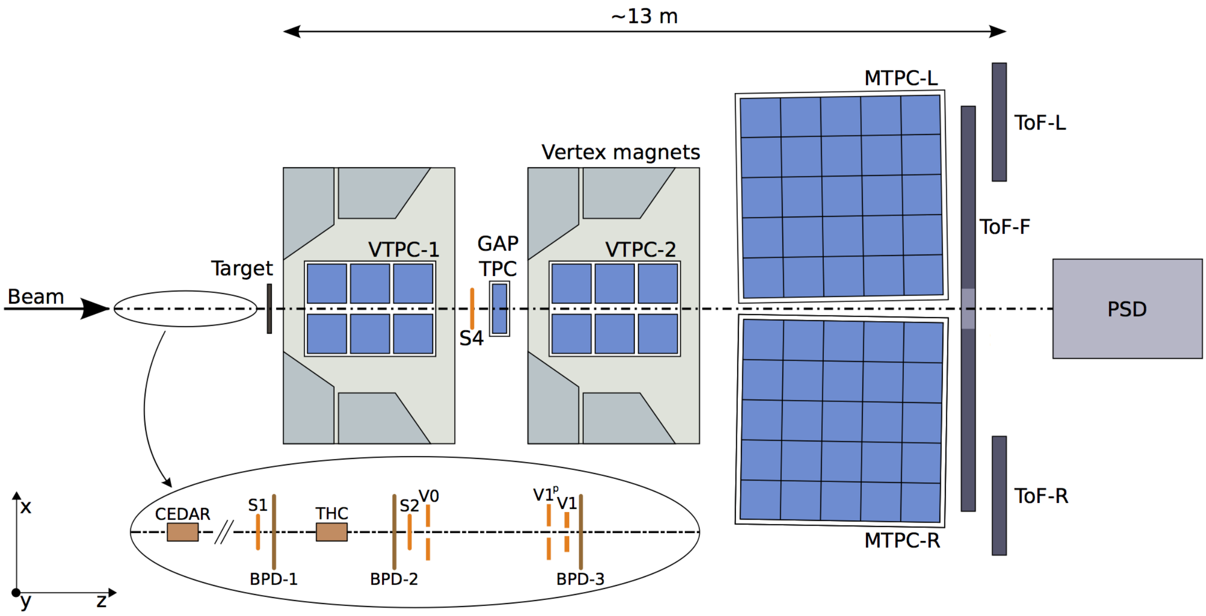

Figure 1: The schematic top-view layout of the NA61/SHINE experiment in the configuration used during the 2015 data-taking. The TOF-F was not installed for the data collected for this analysis.

The NA61/SHINE detector [1] is shown in Figure 1. In standard operation, it comprises four large Time Projection Chambers (TPCs) and a Time of Flight (ToF) system allowing NA61/SHINE to make spectral measurements of produced hadrons. Two of the TPCs, Vertex TPC 1 (VTPC-1) and Vertex TPC 2 (VTPC-2), are contained within superconducting magnets, capable of generating a combined maximum bending power of 9 T·m. However these magnets were not operational during the 2015 run presented here. Downstream of the VTPCs are the Main TPC Left (MTPC-L) and Main TPC Right (MTPC-R). Additionally, a smaller TPC, the Gap TPC (GTPC), is positioned along the beam axis between the two VTPCs. The forward Time-of-Flight (ToF-F) was not installed in 2015, but the two side ToF-Left and ToF-Right walls were present. The Projectile Spectator Detector (PSD), a forward hadron calorimeter, sits downstream of the ToF system.

The most critical systems for the analyses of the 2015 data presented here are the trigger system and the Beam Position Detectors (BPDs). The NA61/SHINE trigger system uses two scintillator counters (S1 and S2) to trigger on beam particles. The S1 counter provides the start time for all counters. Three veto scintillation counters ($V0$, $V1$ and $V1^p$) each with a 1 cm diameter hole are used to remove divergent beam particles upstream of the target. The S4 scintillator with a 1 cm radius sits downstream of the target and is used to determine whether or not an interaction has occurred. A Cherenkov Differential Counter with Achromatic Ring Focus (CEDAR) [8, 9] and a threshold Cherenkov counter (THC) select beam particles of the desired species. The CEDAR focusses the Cherenkov ring from a beam particle onto a ring of 8 PMTs. The pressure is adjusted so that only particles of the desired species will trigger the PMTs, and typically a coincidence of at least 6 PMTs is required to tag a particle for the trigger. Pressure scans of the CEDARs are shown in Figure 2. For these 2015 data at 31 GeV/c the beam was composed of approximately 87% pions, 11% protons, and 2% kaons. At 60 GeV/c the beam was composed of approximately 74% pions, 23% protons, and 3% kaons.

The beam particles are selected by defining the beam trigger (T_{beam}) as the coincidence of $S1 \wedge S2 \wedge \overline{V0} \wedge$

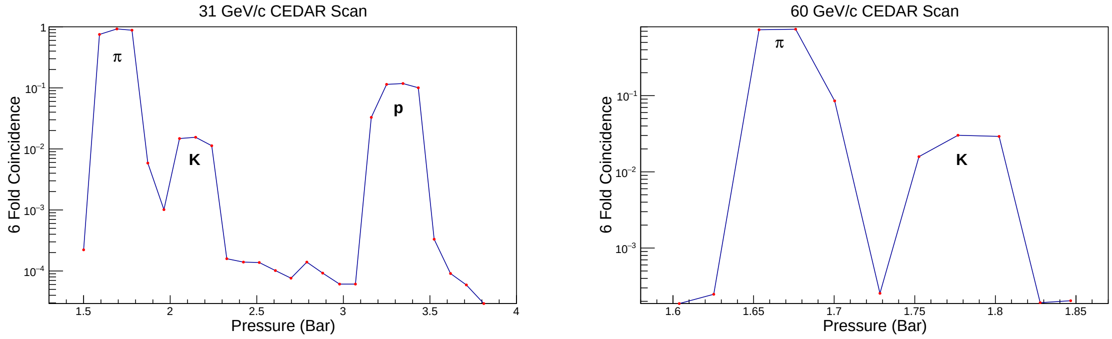

Figure 2: CEDAR pressure scans for the 31 GeV/c beam ($left$) and the 60 GeV/c beam ($right$). The vertical axis shows the fraction of beam particles that fires at least 6 of the 8 CEDAR PMTs.

$\overline{V1} \wedge \overline{V1^p} \wedge CEDAR \wedge \overline{THC}$. The interaction trigger ($T_{\rm int}$) is defined by the coincidence of $T_{\rm beam} \wedge \overline{S4}$ to select beam particles which have interacted with the target. A correction factor will be discussed in detail in Section 5.1 to correct for interactions that hit the S4. Three BPDs, which are proportional wire chambers, are located 30.39 m, 9.09 m, and 0.89 m upstream of the target and determine the location of the incident beam particle to an accuracy of $\sim$100 μm.

For these 2015 data, the interactions of p, π^+, and K^+ beams were measured on thin carbon and aluminum targets. The carbon target was composed of graphite of density $\rho = 1.84$ g/cm^3 with dimensions of 25 mm (W) x 25 mm (H) x 20 mm (L), corresponding to roughly 4% of a proton-nuclear interaction length. The aluminum target has a density of $\rho = 2.70$ g/cm^3 with dimensions of 25 mm (W) x 25 mm (H) x 14.8 mm (L), corresponding to roughly 3.6% of a proton-nuclear interaction length.

3 Analysis Procedure

3.1 Event selection

Several cuts were applied to events to ensure the purity of the measurement and to control the systematic effects caused by beam divergence. First, the so-called WFA (Wave Form Analyzer) cut was used to remove events in which multiple beam particles pass through the beam line in a small time frame. The WFA determines the timing of beam particles that pass through the S1 scintillator. If another beam particle passes through the beam line close in time to the triggered beam particle, it could cause a false trigger in the S4 scintillator. In order to mitigate this effect, a conservative cut of $\pm$ 2 μs was applied to the time window to ensure that only one particle is allowed to pass through the S1 in a 4 μs time window around the selected beam particle.

The trajectories of the incoming beam particles are measured by three BPDs, located along the beamline upstream of the target as shown in Figure 1. The measurements from the BPDs are especially important for estimating the effects of beam divergence on the cross section measurements. To understand these effects, tracks are fitted to the reconstructed BPD clusters, and the tracks are extrapolated to the S4 plane. The so-called “Good BPD" cut requires that the event includes a cluster in the most-downstream BPD and that a track was successfully fit to the BPDs. Figures 3 and 4 show the resulting BPD extrapolation to the S4 plane for the interactions studied. It can be seen from these figures that the 31 GeV/c beams

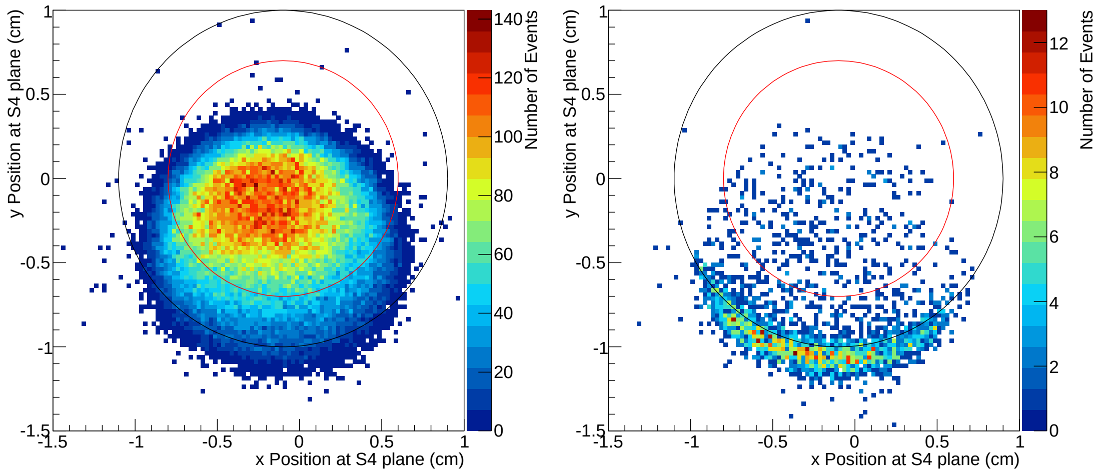

Figure 3: Positions of BPD tracks extrapolated to the S4 plane in Target Removed data runs from the $\pi^+ + \mathrm{C}$ at 31 GeV/c dataset. The measured S4 position is shown as a black circle and the BPD radius cut is shown as a red circle in both figures. ($Left$) Events taken by the beam trigger. ($Right$) Events taken by the interaction trigger.

were much wider than the 60 GeV/c beams. From these figures, it is also evident that the V1 veto counter (which is close to the most downstream BPD) and S4 were not well-aligned. The beam was wide enough that a significant fraction of the beam particles have trajectories missing the S4. This leads to an apparent interaction rate higher than the actual interaction rate. To reduce this effect, a radial cut was applied to the BPD tracks extrapolated to the S4, and this is indicated by the red circles on Figures 3 and 4.

The number of events after the described selection cuts for the interactions: 60 GeV/c K^+ and π^+ and 31 GeV/c π^+ with C and Al targets (Target Inserted) and with the targets removed (Target Removed) are shown in Tables [1 - 3].

Interaction	$\pi^+ + \mathrm{C}$		$\pi^+ + \mathrm{Al}$	
Target	Inserted	Removed	Inserted	Removed
Total	593,176	195,492	534,813	234,302
WFA	591,414	194,969	531,785	233,056
Good BPD	547,297	180,315	491,019	215,181
Radial cut	437,373	142,790	367,240	158,872

Table 1: Event selection table for $\pi^+ + \mathrm{C}$ and $\pi^+ + \mathrm{Al}$ at 31 GeV/c.

4 Interaction trigger cross sections

In general, the probability of a beam particle interaction inside of a thin target is proportional to the thickness L of the target and the number density of the target nuclei n. Thus, the interaction probability P can be defined by taking into account the thin target approximation and by defining the interaction cross section σ

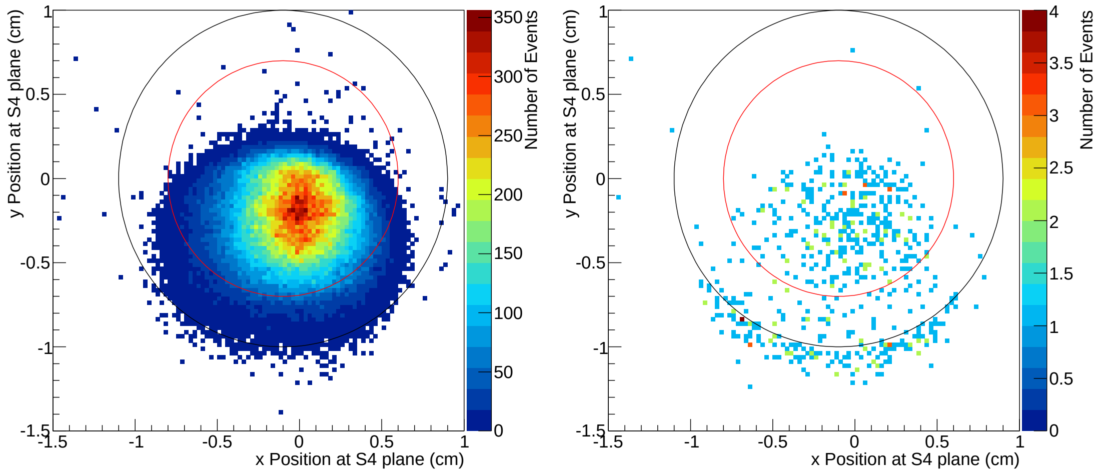

Figure 4: Positions of BPD tracks extrapolated to the S4 plane in Target Removed data runs from the $\pi^+ + \mathrm{C}$ at 60 GeV/c dataset. The measured S4 position is shown as a black circle and the BPD radius cut is shown as a red circle in both figures. $(Left)$ Events taken by the beam trigger. $(Right)$ Events taken by the interaction trigger.

Interaction	$\pi^+ + \mathrm{C}$		$\pi^+ + \mathrm{Al}$	
Target	Inserted	Removed	Inserted	Removed
Total	528,086	246,902	458,800	285,721
WFA	513,449	240,438	447,793	279,031
Good BPD	479,199	224,512	417,369	260,163
Radial cut	462,912	217,080	405,379	252,237

Table 2: Event selection table for $\pi^+ + \mathrm{C}$ and $\pi^+ + \mathrm{Al}$ at 60 GeV/c.

Interaction	$K^+ + \mathrm{C}$		$K^+ + \mathrm{Al}$	
Target	Inserted	Removed	Inserted	Removed
Total	505,525	239,145	338,987	155,796
WFA	503,110	238,024	337,309	155,035
Good BPD	465,832	220,703	312,418	143,502
Radial cut	462,544	218,946	310,482	142,625

Table 3: Event selection table for $K^+ + \mathrm{C}$ and $K^+ + \mathrm{Al}$ at 60 GeV/c.

as:

$$P = \frac{\text{Number of events}}{\text{Number of beam particles}} = n \cdot L \cdot \sigma. \tag{3}$$

The density of nuclei n can be calculated in terms of N_A, ρ, and A, which are Avogadro's number, the material density, and the atomic number, respectively.

The counts of beam and interaction triggers as described in Sec. 2 can be used to estimate the trigger probability as follows:

$$P_{\text{Tint}} = \frac{N(T_{\text{beam}} \wedge T_{\text{int}})}{N(T_{\text{beam}})}, \tag{4}$$

where $N(T_{beam})$ is the number of beam events passing the event selection cuts and $N(T_{beam} \wedge T_{int})$ is the number of selected beam events which also have an interaction trigger. In order to correct for events where the beam particle interacts outside of the target, data were also taken with the target removed from the beam (Target Removed). Figure 5 shows an example of the trigger interaction probabilities for each run for the $\pi^+ + \text{C}$ at 60 GeV/c dataset. Table 4 gives the total trigger interaction probabilities for the data sets used in this paper for both the Target Inserted and Target Removed data. The kaon target removed interaction probabilities are larger than those for pions due to the fact that $\sim 1\%$ of the beam kaons will decay between BPD 3 and S4.

Taking into account the trigger probabilities with the target inserted (I) and the target removed (R), $P^{\text{I}}_{\text{Tint}}$ and $P^{\text{R}}_{\text{Tint}}$, the interaction probability P_{int} can be obtained:

$$P_{\text{int}} = \frac{P^{\text{I}}_{\text{Tint}} - P^{\text{R}}_{\text{Tint}}}{1 - P^{\text{R}}_{\text{Tint}}}. \tag{5}$$

Equation 3 leads to the definition of the trigger cross section σ_{trig}, by using P_{int} and the effective target length L_{eff}, which accounts for the exponential beam attenuation:

$$\sigma_{\text{trig}} = \frac{A}{\rho L_{\text{eff}} N_{\text{A}}} \cdot P_{\text{int}}. \tag{6}$$

The effective target length can be calculated using the absorption length,

$$L_{\text{eff}} = \lambda_{\text{abs}}(1 - e^{-L/\lambda_{\text{abs}}}), \tag{7}$$

with

$$\lambda_{\text{abs}} = A/(\rho N_{\text{A}} \sigma_{\text{trig}}). \tag{8}$$

By simplifying Equations 6, 7, and 8, one can obtain σ_{trig} as

$$\sigma_{\text{trig}} = -\frac{A}{\rho L N_{\text{A}}} \ln(1 - P_{\text{int}}). \tag{9}$$

5 Correction factors

5.1 S4 trigger correction factors

The trigger cross section contains the interactions where the resulting particles miss the S4 scintillator counter that is downstream of the target. But even when there has been a production or quasi-elastic interaction in the target, there is a possibility that a forward-going particle will strike the S4 counter. Moreover, not all elastically scattered beam particles strike the S4. Corrections must be applied to the

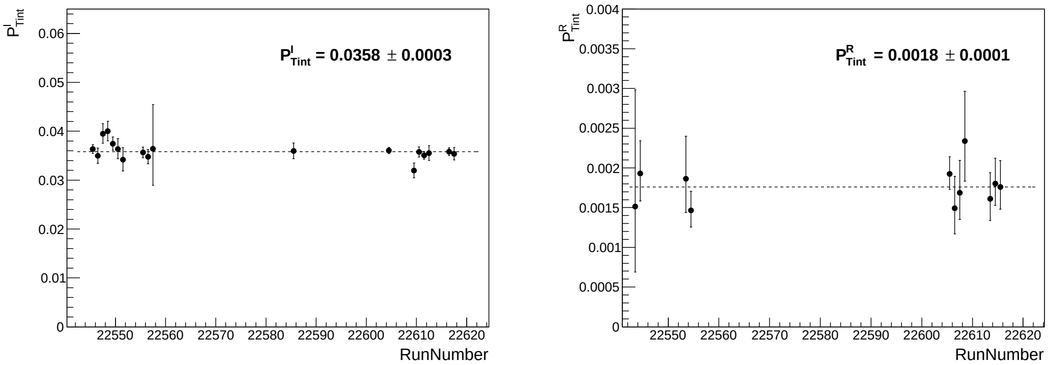

Figure 5: Trigger interaction probabilities for $\pi^+ + \mathrm{C}$ at 60 GeV/c dataset. ($Left$) Target Inserted dataset. ($Right$) Target Removed dataset.

Interaction	p (GeV/c)	$P^{\mathrm{I}}_{\mathrm{Tint}}$	$P^{\mathrm{R}}_{\mathrm{Tint}}$
$\pi^+ + \mathrm{C}$	31	0.0407 ± 0.0003	0.0025 ± 0.0001
$\pi^+ + \mathrm{Al}$	31	0.0391 ± 0.0003	0.0029 ± 0.0001
$\pi^+ + \mathrm{C}$	60	0.0358 ± 0.0003	0.0018 ± 0.0001
$\pi^+ + \mathrm{Al}$	60	0.0320 ± 0.0003	0.0018 ± 0.0001
$K^+ + \mathrm{C}$	60	0.0394 ± 0.0003	0.0103 ± 0.0002
$K^+ + \mathrm{Al}$	60	0.0373 ± 0.0004	0.0103 ± 0.0003

Table 4: Trigger Interaction probabilities in data. For each configuration, the observed probabilities for Target Inserted and Target Removed data are given.

trigger cross section to account for these effects. Combining Equations 1 and 2, the trigger cross section can be related to the production cross section through Monte Carlo (MC) correction factors as follows:

$$\sigma_{\mathrm{trig}} = \sigma_{\mathrm{prod}} \cdot f_{\mathrm{prod}} + \sigma_{\mathrm{qe}} \cdot f_{\mathrm{qe}} + \sigma_{\mathrm{el}} \cdot f_{\mathrm{el}} \ , \tag{10}$$

where f_{prod}, f_{qe}, and f_{el} are the fractions of production, quasi-elastic, and elastic events that miss the S4 counter. σ_{qe} and σ_{el} are also estimated from Monte Carlo. Equation 10 can be rewritten to obtain σ_{prod} and σ_{inel} as:

$$\sigma_{\mathrm{prod}} = \frac{1}{f_{\mathrm{prod}}}(\sigma_{\mathrm{trig}} - \sigma_{\mathrm{qe}} \cdot f_{\mathrm{qe}} - \sigma_{\mathrm{el}} \cdot f_{\mathrm{el}}) \tag{11}$$

and

$$\sigma_{\mathrm{inel}} = \frac{1}{f_{\mathrm{inel}}}(\sigma_{\mathrm{trig}} - \sigma_{\mathrm{el}} \cdot f_{\mathrm{el}}). \tag{12}$$

A GEANT4 detector simulation [10, 11, 12] was used to estimate the MC correction factors discussed above. The FTFP_BERT physics list with GEANT4 version of 10.2.p03 was used to estimate correction factors as presented in Table 5.

Interaction	p	Monte Carlo Correction Factors					
	(GeV/c)	σ_{el} (mb)	f_{el}	σ_{qe} (mb)	f_{qe}	f_{prod}	f_{inel}
$\pi^+ + \mathrm{C}$	31	55.5	0.734	18.8	0.946	0.989	0.985
$\pi^+ + \mathrm{Al}$	31	114.5	0.745	29.7	0.949	0.990	0.987
$\pi^+ + \mathrm{C}$	60	54.0	0.289	16.4	0.811	0.967	0.952
$\pi^+ + \mathrm{Al}$	60	110.0	0.232	25.7	0.814	0.969	0.956
$K^+ + \mathrm{C}$	60	18.1	0.323	14.5	0.821	0.990	0.975
$K^+ + \mathrm{Al}$	60	44.6	0.183	23.5	0.821	0.990	0.997

Table 5: Monte Carlo correction factors.

5.2 Beam composition correction factors

In the case of π^+ beams, a correction must also be applied for the beam composition. This is because the CEDAR and threshold Cherenkov detectors do not have the power to completely discriminate positrons from pions at 31 GeV/c and 60 GeV/c as shown in [8, 9]. This problem is worse for 60 GeV/c. Fortunately, it was possible to estimate the amount of positron contamination with special maximum field runs and with the PSD. During the neutrino data-taking in 2016, a special maximum field data run was taken. The magnets were set to the 9·m field setting such that the 60 GeV/c beam was bent into the MTPC-L. Both PSD and dE/dx data were recorded. Data were also taken with upstream lead absorbers in and out of the beam leading to different levels of positron contamination.

The PSD is usually used as a hadron calorimeter for heavy ion interactions, but it can also be used to help discriminate between low mass hadrons and positrons. The electromagnetic radiation length of positrons is much smaller than the hadronic radiation length of pions at 31 GeV/c and 60 GeV/c. Therefore, the positrons tend to deposit all of their energy in the first two sections (longitudinal layers) of the PSD, while pions penetrate deeper into the PSD calorimeter. By only selecting beam particles that penetrate deep into the PSD, a pure pion sample is obtained. This sample is used to determine the parameters of the pion dE/dx gaussian distribution μ_π and σ_π.

To determine the positron and π^+ compositions of the beam, a sum of two gaussians is fit to the dE/dx data. The distance between the positron and pion means and the ratio of the positron and pion spread are determined from a Bethe Bloch model. Therefore, only the amplitudes of the pion and positron distributions are allowed to float. The positron contamination was determined to be $2\%\pm2\%$ for the 60 GeV/c beam. Figure 6 shows the resulting fit to the maximum field data.

Finally, the effect of the positrons on the trigger cross section must be estimated. The same GEANT4 MC simulation is used to determine this effect. Positrons were simulated with a carbon target, an aluminum target and with the targets removed to determine the $P^{\mathrm{I}}_{\mathrm{Tint}}$ and $P^{\mathrm{R}}_{\mathrm{Tint}}$ rates. In the case of 60 GeV/c pion interactions, a correction is applied to the measured values of $P^{\mathrm{I}}_{\mathrm{Tint}}$ and $P^{\mathrm{R}}_{\mathrm{Tint}}$:

$$P^{\mathrm{corr}}_{\mathrm{Tint}} = (P_{\mathrm{Tint}} - P_e \cdot f_e)/f_\pi \quad (\mathrm{Target\ I, R})\ , \tag{13}$$

where $f_e = 0.02$ and $f_\pi = 0.98$. The resulting corrections applied to σ_{prod} (σ_{inel}) are +2.2% (+2.1%) for $\pi^+ + \mathrm{C}$ at 60 GeV/c and +1.8% (1.7%) for $\pi^+ + \mathrm{Al}$ at 60 GeV/c.

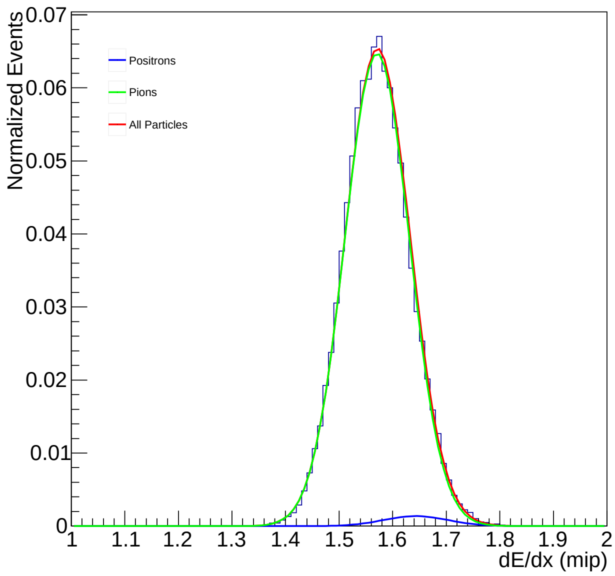

Figure 6: The binned data shows the dE/dx distribution of the maximum field dataset for the 60 GeV/c π^+ beam. Overlaid is the sum of gaussians fit to the histogram as well as the individual π^+ and e^+ components. From this fit, the positron contribution was estimated to be 2%.

In the case of 31 GeV/c, the potential for positron contamination was reduced by requiring that the CEDAR had a more stringent 7-fold coincidence signal. No special data run was undertaken with the 31 GeV/c beam to measure the positron contamination, so no correction is applied. But this contamination will be taken into account later as an asymmetric systematic uncertainty.

For the pion beams at both 31 GeV/c and 60 GeV/c, a small number of muons are also present in the beam due to the decays of pions upstream of the target, and the CEDAR cannot completely distinguish these from pions. Many of these muons will emerge at an angle and will strike the veto counters, but simulations at both momenta show the muon fraction that will pass the veto counters and trigger our beam counters is about 1.5±0.5% of the pion beam. A correction for the muon component of the beam is applied to the 31 GeV/c, and 60 GeV/c pion beam interactions.

For the kaon beam, any kaons that decay upstream of the CEDAR will not satisfy the beam selection and will not be selected as good beam particles. Only kaon decays downstream of the CEDAR where the decay products are headed towards the S4 will pass the beam selection and “Good BPD" cut. It has been estimated that only 0.1% of the CEDAR-tagged kaons will decay with decay products that pass these cuts. Therefore no correction is applied for kaon decays in the beamline.

6 Systematic uncertainties

6.1 Target density uncertainty

The uncertainty on the target density affects the calculation of the trigger cross section as shown in Equation 9. The density uncertainty for each target is estimated by calculating the standard deviation of the target densities determined from measurements of the mass and dimensions of the machined target samples. A 0.65% uncertainty on the density of carbon and a 0.29% uncertainty on the density of aluminum were used. The uncertainties on the densities are then propagated to the uncertainties on the cross section results for all of the interactions studied. The target density uncertainties are included in the breakdowns in the systematic uncertainties for the production and inelastic cross sections presented in Tables 6 and 7.

6.2 Out-of-target interactions

As shown in Equation 5, the measured interaction rates are corrected for interactions occurring outside of the target by measuring the trigger rates with the target both inserted and removed. Switching between target “I” and “R” is achieved by moving the target holder out of the path of the beam. To look for possible additional systematic effects, during the 2015 data-taking two special runs were undertaken as a cross-check. These data were taken with the target holder in the “I” position and with the target holder in the “R” position, but with no target attached. The data were taken with 31 GeV/c and 60 GeV/c π^+. With no additional out-of-target effects, the target holder data (both the “I" and “R” runs) should exhibit the same trigger probability as the target removed data.

In the case of the 31 GeV/c target holder data, there was no significant difference between the trigger probability of the empty target holder data and the target removed data. However, in the case of the 60 GeV/c data run, a high trigger probability in the target holder “I” run was observed. These out-of-target interactions may be related to the beam conditions during those runs. An asymmetric uncertainty was assigned for the 60 GeV/c interactions. These uncertainties are included in the breakdowns of the systematic uncertainties for the production and inelastic cross sections presented in Tables 6 and 7.

6.3 S4 size uncertainty

Another systematic uncertainty comes from the uncertainty in the size of the S4 scintillator. The diameter of the S4 was measured with calipers to be $D_{\mathrm{S4}} = 20.06 \pm 0.40$ mm.

In order to propagate this uncertainty to σ_{inel} and σ_{prod}, two additional MC simulation samples with the S4 diameter modified to be 2.04 and 1.96 cm were generated. After obtaining the new S4 correction factors f_{inel}, f_{prod}, f_{qe}, and f_{el}, σ_{inel} and σ_{prod} were recalculated. The maximum and minimum values of σ_{inel} and σ_{prod} obtained from these MC simulation samples are taken as the upper and lower limits on the S4 size uncertainty. Uncertainties related to the S4 size are included in the breakdowns of the systematic uncertainties for the production and inelastic cross sections presented in Tables 6 and 7.

6.4 S4 efficiency

The uncertainty on the S4 scintillator efficiency was estimated using Target Removed data. GTPC tracks are extrapolated to the S4 plane and matched with beam tracks which pass the “Good BPD" requirement. Then, the S4 inefficiency was obtained by calculating the trigger probability as defined in Eq. (4) for events which have matched tracks. Previous NA61/SHINE analyses have found that S4 inefficiency is negligibly small [13] and this analysis also found no S4 inefficiency. The S4 inefficiency is concluded to be less than 0.1% and neither an uncertainty nor a correction relating to the S4 scintillator efficiency is applied to the results.

6.5 Beam composition uncertainty

As was mentioned in Section 5.2, for interactions with the 60 GeV/c π^+ beam, a correction was applied to reflect the small amount of positrons in the beam. To be conservative, 100% of this correction is assumed as a systematic uncertainty. For π^+ at 31 GeV/c, no correction is applied, but an uncertainty is reported accounting for a 1% positron contamination. This results in an asymmetric uncertainty of $[+1.9, -0.0]$ mb for $\pi^+ + \mathrm{C}$ at 31 GeV/c and $[+2.7, -0.0]$ mb for $\pi^+ + \mathrm{Al}$ at 31 GeV/c.

As was also mentioned in Section 5.2, the muon fraction in the pion beam is estimated to be 1.5% for both the 31 GeV/c and 60 GeV/c π^+ beams and a correction was applied. An uncertainty of 0.5% is applied to this correction.

The CEDAR counter has a high purity of identifying kaons using a 6-fold coincidence. Kaons are well-separated from pions and protons. The lower limit on the purity of the kaon beam has been calculated to be 99.4% according to the CEDAR gas pressure scan data. The estimated systematic error from this source is applied to the total systematic uncertainty.

Uncertainties related to uncertainty in the beam composition are summarized in the breakdowns of the systematic uncertainties for the production and inelastic cross sections presented in Tables 6 and 7.

6.6 Model uncertainties

The S4 correction factors f_{prod}, f_{inel}, f_{el} and f_{qe} as well as the cross sections σ_{qe} and σ_{el} were estimated with GEANT4 MC simulations using the FTFP_BERT physics list. In order to estimate the model uncertainties associated with these correction factors, the correction factors were recalculated with three additional physics lists: QBBC, QGSP_BERT and FTF_BIC. These physics lists use different underlying physics models in GEANT4's internal calculation of rates for different interaction processes. Using these additional physics lists, the model dependency on the total cross section measurements was studied. For each physics list, σ_{inel} and σ_{prod} is recalculated with the new correction factors. The maximum and minimum values of σ_{inel} and σ_{prod} from the four physics lists are taken as the upper and lower limits to the model uncertainties in the total cross section results.

These model uncertainties are presented along with the systematic uncertainties associated with the production and inelastic cross sections in Tables 6 and 7.

		Systematic uncertainties for σ_{prod} (mb)						
Interaction	p (GeV/c)	Density	Out-of-target	S4 Size	Beam Purity	MC Stat.	Total Syst. Uncer.	Model Uncer.
$\pi^+ + \text{C}$	31	±1.4	–	$\pm^{0.9}_{0.7}$	$\pm^{2.3}_{1.1}$	±0.3	$\pm^{2.8}_{2.0}$	$\pm^{1.1}_{0.4}$
$\pi^+ + \text{Al}$	31	±1.2	–	$\pm^{1.8}_{1.8}$	$\pm^{3.5}_{2.2}$	±0.6	$\pm^{4.2}_{3.1}$	$\pm^{3.9}_{0.6}$
$\pi^+ + \text{C}$	60	±1.3	$\pm^{0.0}_{1.2}$	$\pm^{1.4}_{1.3}$	$\pm^{4.0}_{3.8}$	±0.3	$\pm^{4.4}_{4.4}$	$\pm^{0.4}_{1.4}$
$\pi^+ + \text{Al}$	60	±1.1	$\pm^{0.0}_{4.3}$	$\pm^{2.4}_{2.8}$	$\pm^{6.4}_{6.1}$	±0.6	$\pm^{6.9}_{8.1}$	$\pm^{0.8}_{0.7}$
$K^+ + \text{C}$	60	±0.8	±0.6	$\pm^{0.3}_{0.3}$	$\pm^{0.3}_{0.3}$	±0.1	$\pm^{1.1}_{1.1}$	$\pm^{0.2}_{2.9}$
$K^+ + \text{Al}$	60	±1.1	±1.2	$\pm^{0.5}_{0.5}$	$\pm^{0.5}_{0.5}$	±0.1	$\pm^{1.8}_{1.8}$	$\pm^{0.1}_{4.1}$

Table 6: Breakdown of systematic uncertainties for production cross section measurements with the NA61/SHINE data.

		Systematic uncertainties for σ_{inel} (mb)						
Interaction	p (GeV/c)	Density	Out-of-target	S4 Size	Beam Purity	MC Stat.	Total Syst. Uncer.	Model Uncer.
$\pi^+ + \text{C}$	31	±1.4	–	$\pm^{0.9}_{0.7}$	$\pm^{2.3}_{1.1}$	±0.3	$\pm^{2.8}_{2.0}$	$\pm^{1.2}_{0.4}$
$\pi^+ + \text{Al}$	31	±1.2	–	$\pm^{1.8}_{1.8}$	$\pm^{3.6}_{2.2}$	±0.6	$\pm^{4.2}_{3.2}$	$\pm^{4.0}_{0.6}$
$\pi^+ + \text{C}$	60	±1.3	$\pm^{0.0}_{1.3}$	$\pm^{1.4}_{1.2}$	$\pm^{4.1}_{4.0}$	±0.3	$\pm^{4.5}_{4.6}$	$\pm^{0.3}_{3.9}$
$\pi^+ + \text{Al}$	60	±1.1	$\pm^{0.0}_{4.3}$	$\pm^{2.5}_{2.8}$	$\pm^{6.4}_{6.2}$	±0.6	$\pm^{7.0}_{8.1}$	$\pm^{1.1}_{0.8}$
$K^+ + \text{C}$	60	±0.8	±0.6	$\pm^{0.3}_{0.4}$	$\pm^{0.3}_{0.3}$	±0.1	$\pm^{1.1}_{1.1}$	$\pm^{0.1}_{2.3}$
$K^+ + \text{Al}$	60	±1.1	±1.2	$\pm^{0.6}_{0.5}$	$\pm^{0.5}_{0.5}$	±0.1	$\pm^{1.8}_{1.8}$	$\pm^{0.1}_{3.1}$

Table 7: Breakdown of systematic uncertainties for inelastic cross section measurements with the NA61/SHINE data.

7 Results

Several production cross sections have been measured in this analysis: $\pi^+ + \text{C}$ ($\pi^+ + \text{Al}$) at 31 GeV/c is found to be 158.3 mb (310.4 mb), $\pi^+ + \text{C}$ ($\pi^+ + \text{Al}$) at 60 GeV/c is found to be 171.6 mb (321.0 mb), and $K^+ + \text{C}$ ($K^+ + \text{Al}$) at 60 GeV/c is found to be 144.5 mb (284.0 mb), respectively. Statistical, systematic, and physics model uncertainties are estimated separately and are summarized in Table 8. π^+ and K^+ at 60 GeV/c measurements are compared with the results of Carrol et al. [14] as shown in Figure 7.

Several inelastic cross sections have also been determined in this analysis: $\pi^+ + \text{C}$ ($\pi^+ + \text{Al}$) at 31 GeV/c is found to be 177.0 mb (340.0 mb), $\pi^+ + \text{C}$ ($\pi^+ + \text{Al}$) at 60 GeV/c is found to be 188.2 mb (347.0 mb), and $K^+ + \text{C}$ ($K^+ + \text{Al}$) at 60 GeV/c is found to be 159.0 mb (307.5 mb), respectively. Statistical, systematic, and physics model uncertainties are estimated separately and are summarized in Table 9. These measurements are compared with the results of Denisov et al. [15] as shown in Figure 8.

Additionally, a short data run of interactions of 31 GeV/c protons with carbon was analyzed as a cross-check with the previous higher statistics NA61/SHINE total cross section results from the 2009 T2K data run [2]. The total production (total inelastic) cross section was found to be 229.8± 4.4 mb (259.9±4.5 mb) (statistical uncertainty only). These are consistent with the 2009 result of 230.7 mb (258.4 mb).

Interaction	p	Production cross section (mb)				
	(GeV/c)	σ_{prod}	Δ_{stat}	Δ_{syst}	Δ_{model}	Δ_{total}
$\pi^+ + \text{C}$	31	158.3	± 2.0	$\pm^{2.8}_{2.0}$	$\pm^{1.1}_{0.4}$	$\pm^{3.6}_{2.9}$
$\pi^+ + \text{Al}$	31	310.4	± 4.3	$\pm^{4.2}_{3.1}$	$\pm^{3.9}_{0.6}$	$\pm^{7.2}_{5.3}$
$\pi^+ + \text{C}$	60	171.6	± 1.7	$\pm^{4.4}_{4.4}$	$\pm^{0.4}_{1.4}$	$\pm^{4.7}_{4.9}$
$\pi^+ + \text{Al}$	60	321.0	± 4.0	$\pm^{6.9}_{8.1}$	$\pm^{0.8}_{0.7}$	$\pm^{8.0}_{9.1}$
$K^+ + \text{C}$	60	144.5	± 2.0	$\pm^{1.1}_{1.1}$	$\pm^{0.2}_{2.9}$	$\pm^{2.3}_{3.7}$
$K^+ + \text{Al}$	60	284.0	± 5.1	$\pm^{1.8}_{1.8}$	$\pm^{0.1}_{4.1}$	$\pm^{5.4}_{6.8}$

Table 8: Production cross section measurements with the NA61/SHINE data. The central value as well as the statistical (Δ_{stat}), systematic (Δ_{syst}), and model (Δ_{model}) uncertainties are shown. The total uncertainty (Δ_{total}) is the sum of the statistical, systematic, and model uncertainties in quadrature.

Interaction	p	Inelastic cross section (mb)				
	(GeV/c)	σ_{inel}	Δ_{stat}	Δ_{syst}	Δ_{model}	Δ_{total}
$\pi^+ + \text{C}$	31	177.0	± 2.0	$\pm^{2.8}_{2.0}$	$\pm^{1.2}_{0.4}$	$\pm^{3.6}_{2.9}$
$\pi^+ + \text{Al}$	31	340.0	± 4.4	$\pm^{4.2}_{3.2}$	$\pm^{4.0}_{0.6}$	$\pm^{7.3}_{5.5}$
$\pi^+ + \text{C}$	60	188.2	± 1.8	$\pm^{4.5}_{4.6}$	$\pm^{0.3}_{3.9}$	$\pm^{4.9}_{6.3}$
$\pi^+ + \text{Al}$	60	347.0	± 4.1	$\pm^{7.0}_{8.1}$	$\pm^{1.1}_{0.8}$	$\pm^{8.2}_{9.1}$
$K^+ + \text{C}$	60	159.0	± 2.1	$\pm^{1.1}_{1.1}$	$\pm^{0.1}_{2.3}$	$\pm^{2.4}_{3.3}$
$K^+ + \text{Al}$	60	307.5	± 5.1	$\pm^{1.8}_{1.8}$	$\pm^{0.1}_{3.1}$	$\pm^{5.4}_{6.2}$

Table 9: Inelastic cross section measurements with the NA61/SHINE data. The central value as well as the statistical (Δ_{stat}), systematic (Δ_{syst}), and model (Δ_{model}) uncertainties are shown. The total uncertainty (Δ_{total}) is the sum of the statistical, systematic, and model uncertainties in quadrature.

8 Summary

In summary, the production and inelastic cross sections of π^+ and K^+ on carbon and aluminum targets have been measured with the NA61/SHINE experiment. The production cross section with π^+ beams at 31 GeV/c was measured for the first time with a precision of about 2%. At 60 GeV/c the measured production cross sections are comparable to previous results for π^+ and K^+ and the precision was improved to about 3% and 2%, respectively. Inelastic cross section measurements with π^+ and K^+ beams at 60 GeV/c were measured for first time with precisions of about 3% and 2%, respectively. For the inelastic production cross section for π^+ at 31 GeV/c reasonable agreement with a previous measurement was found. Especially for π^+ beams, the measurements here are limited by positron contamination in the beam and steps will be taken in future data-taking to better limit this uncertainty.

The current uncertainties on the neutrino fluxes in the NuMI neutrino beam at Fermilab from the MINERνA collaboration [16] rely on measurements of the inelastic cross section (which is termed the “absorption" cross section in the MINERνA paper). For π^++C and π^++Al they assumed an uncertainty of 5%, while for the K^++C and K^++Al cross sections they assumed a 10-30% uncertainty, which is significantly larger than the systematic uncertainties determined in this paper. Thus this data will greatly reduce the uncertainty on the neutrino flux prediction in NuMI due to kaon interactions.

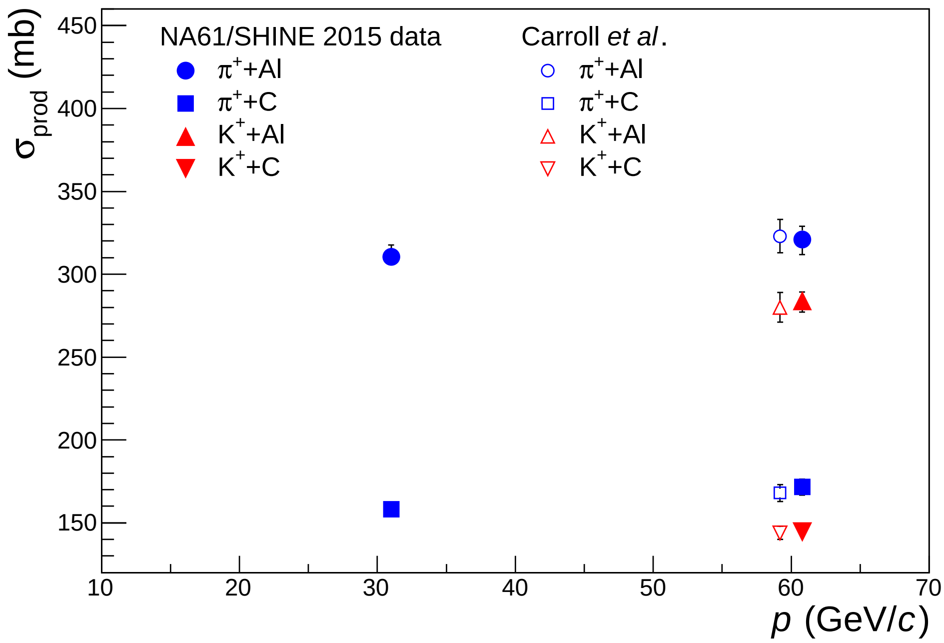

Figure 7: Summary of production cross section measurements. The results are compared to previous results obtained with a beam momentum of 60 GeV/c by Carrol et al. [14] .

Acknowledgments

We would like to thank the CERN EP, BE and EN Departments for the strong support of NA61/SHINE.

This work was supported by the Hungarian Scientific Research Fund (Grants NKFIH 123842–123959), the János Bolyai Research Scholarship of the Hungarian Academy of Sciences, the Polish Ministry of Science and Higher Education (grants 667/N-CERN/2010/0, NN 202 48 4339 and NN 202 23 1837), the Polish National Center for Science (grants 2011/03/N/ST2/03691, 2013/11/N/ST2/03879, 2014/13/N/ST2/ 02565, 2014/14/E/ST2/00018, 2014/15/B/ST2/02537 and 2015/18/M/ST2/00125, 2015/19/N/ST2 /01689, 2016/23/B/ST2/00692), the Russian Science Foundation, grant 16-12-10176, the Russian Academy of Science and the Russian Foundation for Basic Research (grants 08-02-00018, 09-02-00664 and 12-02-91503-CERN), the Ministry of Science and Education of the Russian Federation, grant No. 3.3380.2017/4.6, the National Research Nuclear University MEPhI in the framework of the Russian Academic Excellence Project (contract No. 02.a03.21.0005, 27.08.2013), the Ministry of Education, Culture, Sports, Science and Technology, Japan, Grant-in-Aid for Scientific Research (grants 18071005, 19034011, 19740162, 20740160 and 20039012), the German Research Foundation (grant GA 1480/2-2), the Bulgarian Nuclear Regulatory Agency and the Joint Institute for Nuclear Research, Dubna (bilateral contract No. 4418-1-15/17), Bulgarian National Science Fund (grant DN08/11), Ministry of Education and Science of the Republic of Serbia (grant OI171002), Swiss Nationalfonds Foundation (grant 200020117913/1), ETH Research Grant TH-01 07-3 and the U.S. Department of Energy.

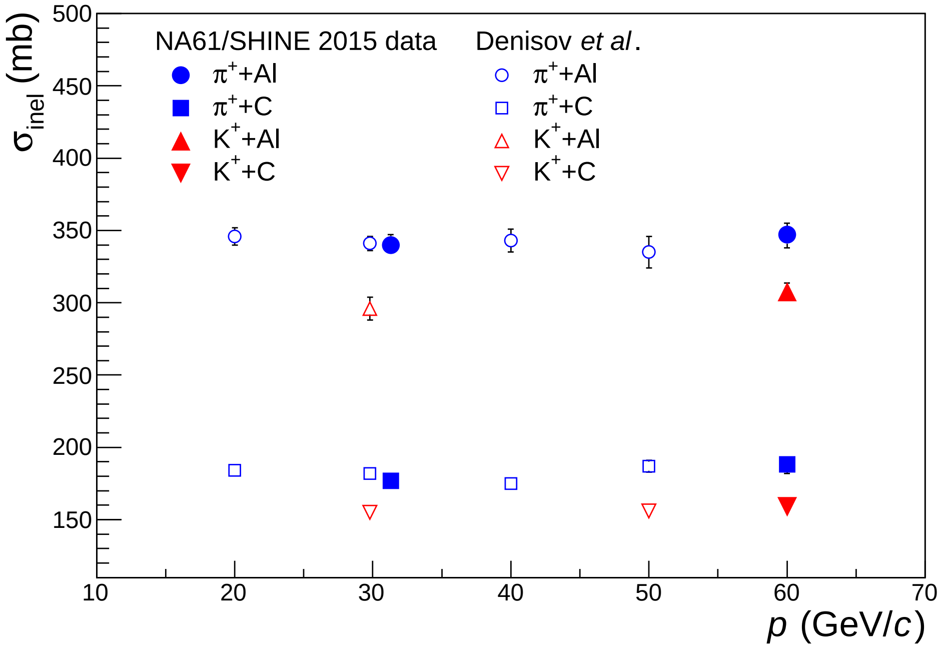

Figure 8: Summary of inelastic cross section measurements. The results are compared to previous results by Denisov et al. [15] .

References

[1] N. Abgrall et al., [NA61 Collab.] JINST 9 (2014) P06005, arXiv:1401.4699 [physics.ins-det].

[2] N. Abgrall et al., [NA61/SHINE Collab.] Eur. Phys. J. C76 no. 2, (2016) 84, arXiv:1510.02703 [hep-ex].

[3] N. Abgrall et al., [NA61/SHINE Collab.] Eur. Phys. J. C76 no. 11, (2016) 617, arXiv:1603.06774 [hep-ex].

[4] K. Abe et al., [T2K Collab.] Nucl.Instrum.Meth. A659 (2011) 106–135.

[5] L. Aliaga et al., [MINERvA Collab.] Nucl. Instrum. Meth. A743 (2014) 130–159, arXiv:1305.5199 [physics.ins-det].

[6] D. S. Ayres et al., [NOvA Collab.] FERMILAB-DESIGN-2007-01 (2007) .

[7] R. Acciarri et al., [DUNE Collab.] arXiv:1512.06148 [physics.ins-det].

[8] C. Bovet, S. Milner, and A. Placci IEEE Trans. Nucl. Sci. 25 (1978) 572–576.

[9] C. Bovet, R. Maleyran, L. Piemontese, A. Placci, and M. Placidi CERN-82-13, CERN-YELLOW-82-13 (1982) .

[10] S. Agostinelli et al., [GEANT4 Collab.] Nucl. Instrum. Meth. A506 (2003) 250–303.

[11] J. Allison et al. IEEE Trans. Nucl. Sci. 53 (2006) 270.

[12] J. Allison et al. Nucl. Instrum. Meth. A835 (2016) 186–225.

[13] N. Abgrall et al., [NA61/SHINE Collab.] Phys. Rev. C84 (2011) 034604, arXiv:1102.0983 [hep-ex].

[14] A. Carroll et al. Phys. Lett. B80 (1979) 319.

[15] S. P. Denisov, S. V. Donskov, Yu. P. Gorin, R. N. Krasnokutsky, A. I. Petrukhin, Yu. D. Prokoshkin, and D. A. Stoyanova Nucl. Phys. B61 (1973) 62–76.

[16] L. Aliaga et al., [MINERvA Collab.] Phys. Rev. D94 no. 9, (2016) 092005, arXiv:1607.00704 [hep-ex]. [Addendum: Phys. Rev.D95,no.3,039903(2017)].